J Mar Sci Technol (2008) 13:24–39
DOI 10.1007/s00773-007-0245-x

ORIGINAL ARTICLE

Comparison of the mariner Schilling rudder and the mariner rudder for VLCCs in strong winds

Vishwanath Nagarajan · Dong Hoon Kang
Kazuhiko Hasegawa · Kenjiro Nabeshima

Received: October 2, 2006 / Accepted: March 20, 2007

Abstract A simulation model of a very large crude carrier (VLCC) with either a mariner type Schilling rudder or a mariner rudder was developed from captive and free-running model tests. Kijima's regression formula was used to predict the hydrodynamic hull forces on the VLCC. To simulate full-scale maneuvering at cruising speed, the constant torque operation of the main engine was assumed. Considering the higher normal lift force and maneuverability of the mariner type Schilling rudder as compared to the mariner rudder, the size of mariner type Schilling rudder is kept smaller as compared to mariner rudder. To compare the efficiency of the two types of rudder system, maneuvering simulations at constant engine torque and course-keeping simulations at various gusting wind speeds and encounter angles were carried out. Based on the simulation results, the two rudder types were compared from the viewpoint of maneuvering and fuel efficiency in windy conditions.

Key words Mariner type Schilling rudder · Constant torque operation · Fuel efficiency

V. Nagarajan · D.H. Kang (✉) · K. Hasegawa
Department of Naval Architecture and Ocean Engineering, Graduate School of Engineering, Osaka University, 2-1 Yamadaoka, Suita 565-0871, Japan
e-mail: Kang_Dong_Hoon@naoe.eng.osaka-u.ac.jp

K. Nabeshima
Japan Hamworthy Co. Ltd., Osaka, Japan

List of symbols

a_H	Ratio of additional lateral force induced on ship hull by rudder action to the rudder force
A_L	Longitudinal projected area of ship above waterline
A_R	Rudder area
A_T	Transverse projected area of ship above waterline
b_i	Amplitude of gustiness of wind
C_b	Block coefficient
C_D	Rudder drag force coefficient
Δc_F	Roughness allowance
c_{FM}	Frictional resistance coefficient of model according to ITTC-1957 formula
c_{FS}	Frictional resistance coefficient of ship according to ITTC-1957 formula
$C_X(\psi_A)$, $C_Y(\psi_A)$, $C_N(\psi_A)$	Fujiwara's wind force coefficient (surge, sway, and yaw)
C_L	Rudder lift force coefficient
C_N	Rudder normal force coefficient
c_{TM}	Resistance coefficient estimated from model experiments
d	Ship's draft
D_P	Propeller diameter
g_R	Gear ratio of engine shaft to propeller shaft
H	Rudder height
I_{ZZ}	Ship's moment of inertia about the Z axis
i_{zz}	Ship's added moment of inertia about the Z axis

J	Propeller advance coefficient
J_{PP}	Polar moment of inertia of propeller
ΔJ_{PP}	Added polar moment of inertia in water
k	Form factor
K_p	Yaw gain constant in the automatic control system
K_T	Propeller open water thrust coefficient
K_i	Path deviation gain constant in the automatic control system
K_q	Propeller open water torque coefficient
k_x	Propeller race amplification factor
L	Ship's length between perpendiculars
L_r	Distance between ship's center of gravity and application of total sway force due to the rudder
m	Ship's mass
m_x	Ship's added mass in the longitudinal direction
m_y	Ship's added mass in the transverse direction
n	Propeller revolutions
N	Sum of yaw moments acting on the ship
N'_β, N'_r, $N'_{\beta\beta}$, N'_{rr}, $N'_{\beta\beta r}$, $N'_{\beta rr}$	Hydrodynamic coefficients for the yaw moment
Q_E	Main engine torque
Q_P	Propeller torque
r	Yaw rate at ship's center
$\dot{r}$	Yaw acceleration at ship's center
s	Propeller slip ratio
S_w	Wetted surface area of ship
$S_z\left(\frac{\omega}{2\pi}\right)$	Wind power spectrum at height z
t	Time
T_d	Yaw rate gain constant in the automatic control system
t_p	Thrust deduction fraction for propeller
t_R	Thrust deduction fraction for rudder
u	Surge velocity at ship's center
U	Ship's resultant velocity
$\dot{U}$	Ship's resultant acceleration
U_A	Wind speed in ship coordinates
$U_{GW}(t)$	Gust wind speed at time t
u_p	Inflow velocity to propeller
u_R	Inflow velocity to rudder in the longitudinal direction
U_W	Wind speed in Earth coordinates at standard reference height of 10.0 m
v	Sway velocity at ship's center
v_R	Inflow velocity to rudder in the transverse direction
w_M	Wake fraction at propeller position (model)
w_R	Wake fraction at rudder position
w_s	Wake fraction at propeller position (ship)
X	Sum of forces acting on the ship in the longitudinal direction
x_G	Distance between ship's center of gravity and ship's center
x'_H	Distance between the center of gravity of ship and the center of additional lateral force, nondimensionalized by ship length
x_R	Longitudinal distance of rudder from ship center
X'_{vr}	Hydrodynamic coefficient for surge force
y_d	Desired ship's off-centerline deviation
y	Actual ship's off-centerline deviation
Y	Sum of forces acting on the ship in the transverse direction
Y'_β, Y'_r, $Y'_{\beta\beta}$, Y'_{rr}, $Y'_{\beta\beta r}$, $Y'_{\beta rr}$	Hydrodynamic coefficients for sway force
α_R	Effective rudder inflow angle
β	Ship's drift angle
$\dot{\beta}$	Rate of change of ship's drift angle
β_R	Ship's drift angle at rudder position
γ_R	Flow rectification coefficient
δ	Rudder angle
δ_0	Rudder angle at which lift force coefficient C_L is zero
δ_i	Phase angle of gustiness of wind
$\delta_{\max}$	Maximum permissible rudder angle
$\dot{\delta}_{\max}$	Maximum permissible rudder turning rate
ε	Wake ratio of rudder and propeller
η	Ratio of propeller diameter to rudder height
η_R	Relative rotative efficiency
η_t	Shaft transmission efficiency
κ_W	Drag coefficient of Davenport spectrum referred to mean velocity at 10.0 m
Λ	Rudder aspect ratio

ρ	Density of water (model scale: fresh water, full scale: sea water)
ρ_A	Density of air
ψ	Ship's heading
δ_d	Ship's desired heading
ψ_A	Wind direction in ship coordinates
δ_W	Wind direction in Earth coordinates
ω	Frequency of wind power spectrum (Radians per second)

1 Introduction

With increases in shipping trade, many ships are being constructed with a large wind area, e.g., very large crude carriers (VLCCs) (in ballast draft), pure car carriers (PCCs), liquefied natural gas (LNG) carriers, and container ships. These ships are easily deviated from their course by wind forces, and so their performance under windy conditions is important. The influence of wind on PCCs has been well studied. Hasegawa et al.,[1] studied PCCs fitted with Schilling rudders and mariner rudders and concluded that the course keeping ability of a PCC improved when fitted with a Schilling rudder. Improving the maneuvering ability of a VLCC by using different rudder systems has also been well studied. Hasegawa et al.,[2] studied a VLCC fitted with a mariner type Super VecTwin rudder and compared its performance with that of a mariner rudder. They concluded that the mariner type Super VecTwin rudder improved the stopping ability of a VLCC, while keeping other maneuvering characteristics the same as those of the mariner rudder. In the mariner type Super VecTwin rudder, a rudder horn is fitted that provides a housing for an additional pintle to support the rudder, thereby reducing the stress on the rudder stock.

VLCCs are noteworthy because of their relatively low cruising speeds and large windage area, especially in the ballast draft condition. Additionally, for VLCCs in the ballast draft condition, the effective rudder area may decrease due to the lower waterline, making the vessel more susceptible to wind forces. VLCCs spend 50% of their voyage time in the ballast draft condition, and so their performance under windy conditions is very important. Spyrou[3] studied the yaw stability of VLCCs in a steady wind and showed that the ship becomes unstable in following winds. However, no studies have yet been done on the influence of rudder type on the maneuvering ability and fuel efficiency of a VLCC. In this article, the performances of the mariner (MR) rudder and the mariner Schilling (MS) rudder are compared from the viewpoint of both maneuvering and fuel efficiency under gusting wind conditions. Mathematical models of a VLCC fitted with an MS rudder or an MR rudder were developed from captive model tests and open water tests on MS rudders and MR rudders. The mathematical model was validated by free-running tests conducted with a model with an MS or MR rudder. An mathematical modeling group (MMG) type model was then used to carry out full-scale simulations under gusting wind conditions for an MS rudder and an MR rudder. Constant torque operation of the main engine was assumed during numerical simulations.

2 Ship model

The principal particulars of the VLCC model ship are shown in Table 1. The model had no appendages and was made of wood. Studs with a depth of 2.0 mm were nailed to the surface of the model ship at 10.0 mm pitch at square station (SS) 9½ and at the midsection of the bulbous bow to stimulate turbulent flow. The model was equipped with a detachable stern that could be changed to test various types of rudders. Two types of rudder, the MS rudder and the MR rudder, were fabricated for the experiments.

The mariner rudder is well known and is not described here. A brief description of the Schilling rudder and mariner Schilling rudder is given. The layout of the Schilling rudder and its cross section is shown in Fig. 1.

Table 1. Principal particulars of the very large crude carrier (VLCC) model

Length (m)	4.0
Breadth (m)	0.667
Loaded draft	
Even keel (m)	0.24
C_b	0.817
Ballast draft	
Forward (m)	0.08
Aft (m)	0.15
C_b	0.776
Propeller	
Diameter (m)	0.12
Pitch (m)	0.096
Blades	5

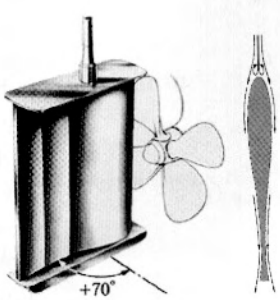

Fig. 1. Perspective view and section of Schilling rudder

The unique profile of the Schilling rudder incorporates a rounded leading edge and a fishtail trailing edge. The Schilling rudder is well known for utilizing the propeller slipstream to achieve an efficient "side thrust" effect at the ship's stern, with operating angles up to 70°. However, at cruising speed, generally the maximum angle of the MS rudder is 35°, and at maneuvering speed it is 70°. Since, fuel consumption calculations are carried out at cruising speed, the maximum rudder angle considered here is 35°. The Schilling rudder is also characterized by end plates fitted to the top and bottom of the rudder. Tachi and Endo[4] showed that the normal force coefficient of a Schilling rudder is higher than that of a mariner rudder because of end plate effects. They also showed that for the Schilling rudder, the stall effect on the normal force coefficient is reduced because of the shape of rudder section.

For VLCCs, rudder forces and moments are high, and a spade type Schilling rudder will require large diameter rudder stock. Large diameter rudder stock will require a larger rudder section to accommodate the stock. So in order to keep the optimum shape of rudder section, a variant of the Schilling rudder called the mariner Schilling rudder is proposed. The mariner Schilling rudder incorporates a rudder horn that provides housing for a pintle to support the rudder. The stresses on the rudder stock are thereby reduced and so its diameter can also be decreased, allowing an optimum rudder section to be designed. The mariner Schilling rudder is fitted with end plates to the top and bottom. The layout of the MS rudder and the MR rudder in a VLCC is shown in Fig. 2.

The MS rudder is characterized by a high normal lift force. It is well established that all types of rudders generate high lift forces in the propeller slipstream. For efficient utilization of the propeller slipstream, a smaller MS rudder is fitted in the propeller slipstream. However, such an optimum arrangement is not possible with an MR rudder, because to keep sufficient maneuvering ability a large rudder is required, the span of which exceeds the propeller diameter, and thereby is larger than the propeller slipstream. From Fig. 2 it can be observed that the depth of the MR rudder is greater than that of the MS rudder. In the ballast condition, part of the MR rudder projects out of water, resulting in a loss of rudder lift force. However, the effective rudder area of the MR rudder is always higher than that of the MS rudder, both in ballast and loaded conditions. The effective area of the MS rudder remains the same at ballast draft and at loaded draft. The particulars of the MR rudder and the MS rudder are shown in Table 2. The reduction in the effective rudder area and lift coefficient of the MR rudder in the ballast condition can be seen.

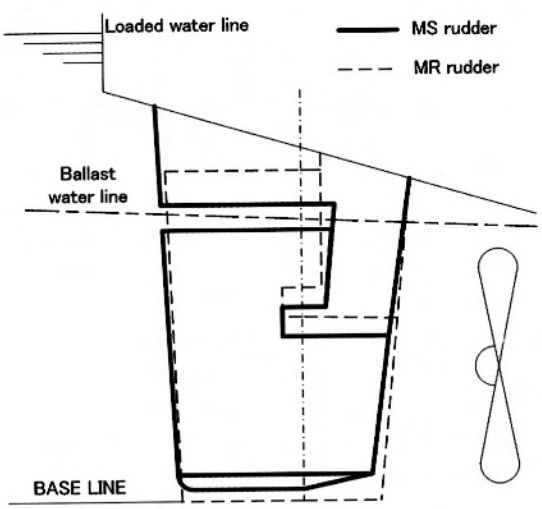

Fig. 2. Layout of mariner (*MR*) and mariner Schilling (*MS*) rudder

3 Captive model experiments

3.1 Resistance tests

Resistance tests with the model were carried out both with an MR rudder and an MS rudder in the Froude number range 0.096–0.144, corresponding to towing speeds of 0.6–0.9 m/s. The propeller was removed during the tests and the shaft end fitted with a fair water cap. The model test results are shown in Fig. 3, and it is observed that the resistance of the ship with an MS rudder or an MR rudder is almost same.

The form factor (k) was estimated from the model test results. Because of the low speed of the vessel, the wave-making resistance component was small. Therefore, for full-scale simulations, scale effects were considered only for the frictional resistance component and wave-making resistance was ignored.

3.2 Self-propulsion tests

Self-propulsion tests were carried out to determine the wake fraction (w_M), the relative rotative efficiency(η_R),

Table 2. Particulars of the mariner (MR) rudder and the mariner Schilling (MS) rudder

	MR rudder		
Coefficients	Ballast	Loaded	MS rudder
A_R (m^2)	0.0123	0.0142	0.0112
Λ (Aspect ratio)	1.73	2.01	1.40
C_N (Normal lift coefficient)	1.60	1.80	2.70

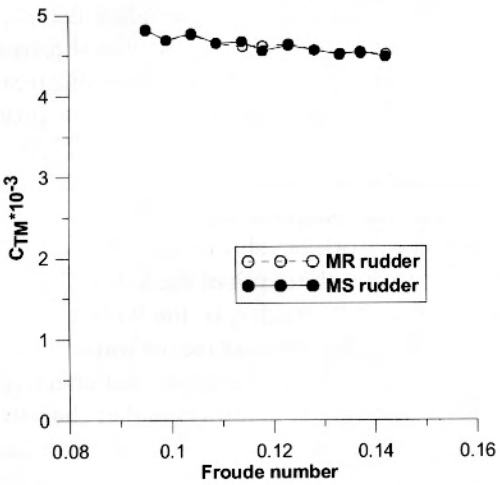

Fig. 3. Resistance test results

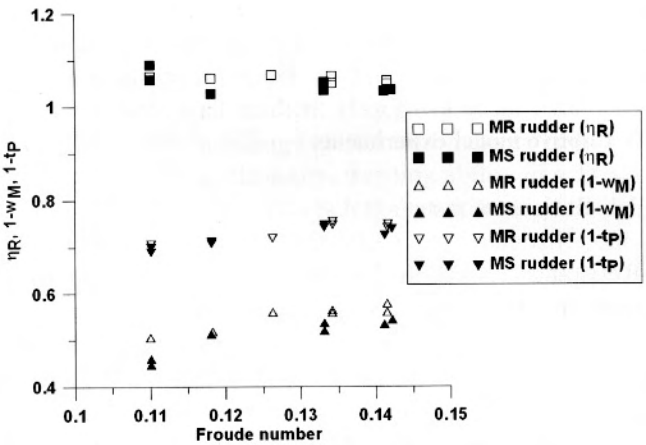

Fig. 4. Interaction coefficients from self-propulsion tests

and the thrust deduction fraction (t_p) of the ship with an MR rudder and an MS rudder. The test results are shown in Fig. 4.

From the test results, it can be seen that the values of the thrust deduction fraction, the wake fraction, and the relative rotative efficiency for the two rudder types are very similar. Hadler and Cheng[5] have also shown that the rudder has an insignificant effect on the wake characteristics in way of propeller, and thus the interaction coefficients for both rudder types are assumed to be same. The wake fraction determined for the model ship was scaled to the full-size ship using ITTC 78 scaling formula[6]:

$$w_s = (t_p + 0.04) + (w_M - t_p - 0.04)\frac{(1+k)c_{FS} + \Delta c_F}{(1+k)c_{FM}} \quad (1)$$

Coefficients of propeller–hull interaction were determined from self-propulsion tests for the model VLCC and are shown in Table 3.

Table 3. Ship–propeller interaction coefficients (model scale)

t_P	0.25
w_M	0.470
η_R	1.065

3.3 Oblique towing tests

Kijima has proposed an MMG type model for predicting hydrodynamic hull forces and moments. Regression formulae have also been proposed to determine the hydrodynamic coefficients based on model tests of several ship types for different loading conditions, e.g., even keel, trim.[7] The range of block coefficient values (C_b) of the model ships used by Kijima was 0.5717–0.8232. Oblique towing tests at full load draft were carried out to determine the hydrodynamic forces, and these were compared with Kijima's model. The Froude number and towing speed were 0.141 and 0.88 m/s, respectively. During the tests, the propeller was removed from the shaft and the shaft end was fitted with a fair water cap. The test results are shown in Fig. 5.

It can be seen that the hydrodynamic hull force and moment for a ship with an MS rudder and an MR rudder are nearly the same. The slight difference is caused by the skeg that is fitted with the rudder horn for the MS rudder. Additionally, it can be observed that Kijima's model well represents the trend of the hydrodynamic moment; however, a slight variation is noted in the prediction of the hydrodynamic sway force.

3.4 Open water rudder tests

When the dimensions of the MS rudder and the MR rudder are the same, the normal force coefficient for the MS rudder can be expressed from that of MR rudder by multiplying it by constant factor.[8] In this article, the MR rudder and the MS rudder have different sizes and aspect ratios. The normal lift force coefficients (C_N) for the MS rudder and MR rudder were determined from open water tests. The open water tests were carried out at a water inflow speed of 1.0 m/s and the Reynolds number range was 1.0–1.1 × 10^5. The results of the open water tests are shown in Fig. 6. The MS rudder has a lift force coefficient (C_L) of ±1.0 at ±22°, and sharp stalls are observed beyond this point, for both port and starboard rudder angles. The MR rudder has smaller C_L values of ±0.65 at the same stall angle for port and starboard helm angles. The C_L values of the MS rudder were higher than those of the MR rudder for the entire range of helm angles. For small rudder angles, the differences in drag coefficient (C_D) between the MS and MR rudders are not very great. At large rudder angles, the drag coefficient

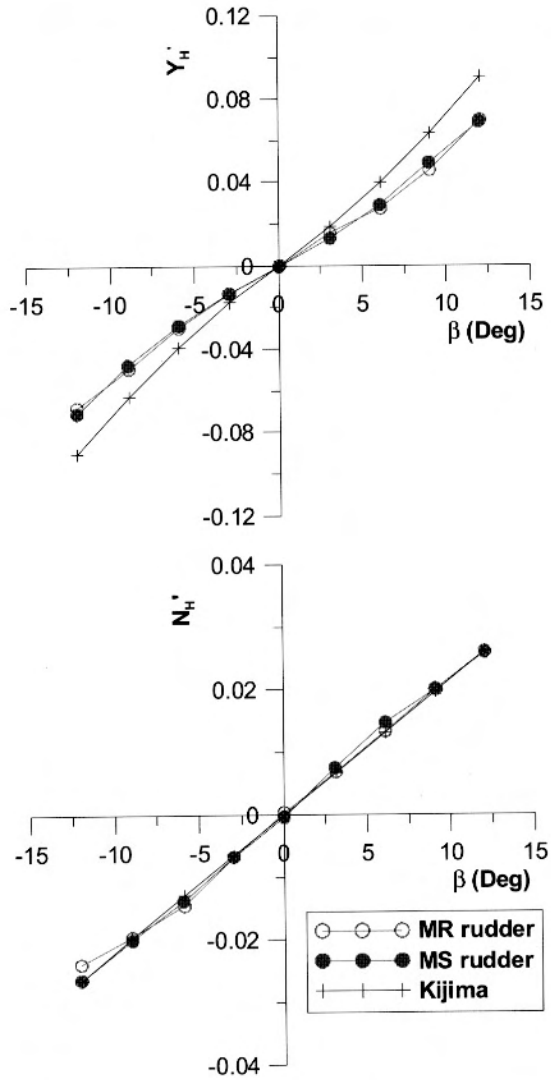

Fig. 5. Hydrodynamic force (Y'_H) and moment (N'_H)

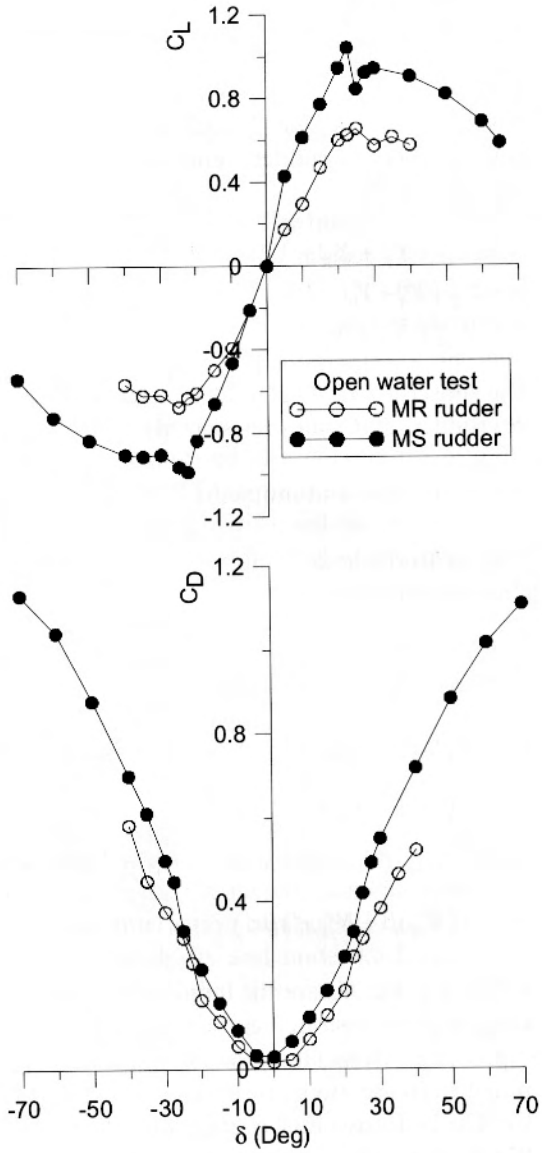

Fig. 6. Lift and drag force coefficients for rudders in the open water condition

of the MS rudder is higher than that for the MR rudder. This is very advantageous because at large rudder angles when the ship speed is reduced and the lift coefficient is increased, a ship with an MS rudder will have superior turning ability compared to one with an MR rudder.

4 Validation of the mathematical model with free-running model experiments

4.1 The coordinate system and the equation of maneuvering motion

A model with three degrees of freedom (surge, sway, and yaw) is considered. The equations for surge, sway, and yaw motions of the ship can be expressed as shown in Eq. 2, based on the coordinate system described in Fig. 7:

$$(m'+m'_x)\left(\frac{L}{U}\right)\left(\frac{\dot{U}}{U}\cos\beta-\dot{\beta}\sin\beta\right)+(m'+m'_y)r'\sin\beta=X'$$

$$-(m'+m'_y)\left(\frac{L}{U}\right)\left(\frac{\dot{U}}{U}\sin\beta+\dot{\beta}\cos\beta\right)+(m'+m'_x)r'\cos\beta=Y'$$

$$(I'_{ZZ}+i'_{ZZ})\left(\frac{L}{U}\right)^2\left(\frac{\dot{U}}{L}r'+\frac{U}{L}\dot{r}'\right)=N' \qquad (2)$$

The primes in Eq. 2 refer to the nondimensional quantities, defined as $m', m'_x, m'_y = \frac{m, m_x, m_y}{\frac{1}{2}\rho L^2 d}$; $I'_{zz}, i'_{zz} = \frac{I_{zz}, i_{zz}}{\frac{1}{2}\rho L^4 d}$;

$X', Y' = \dfrac{X, Y}{\frac{1}{2}\rho L d U^2}$; $N' = \dfrac{N}{\frac{1}{2}\rho L^2 d U^2}$; and $r' = \dfrac{r}{U}L$. The external forces X and Y and moment N consisting of hull, propeller, rudder, and wind components are expressed as:

$$\begin{aligned} X &= X_H + X_P + X_R + X_W \\ Y &= Y_H + Y_R + Y_W \\ N &= N_H + N_R + N_W \end{aligned} \tag{3}$$

The subscripts H, P, R, and W refer to the hull, propeller, rudder, and wind, respectively.

4.2 Hull forces and moments

The hydrodynamic hull forces were modeled using Kijima's formula:

$$\begin{aligned} X_H &= \frac{1}{2}\rho L d U^2 (X'_{vr} v' r') + \frac{1}{2}\rho S_w u^2 c_{TM} \\ Y_H &= \frac{1}{2}\rho L d U^2 \left(Y'_\beta \beta + Y'_r r' + Y'_{\beta\beta}\beta|\beta| + Y'_{rr} r'|r'| \right. \\ &\quad \left. + \left(Y'_{\beta\beta r}\beta + Y'_{\beta rr} r'\right)\beta r'\right) \\ N_H &= \frac{1}{2}\rho L d U^2 \left(N'_\beta \beta + N'_r r' + N'_{\beta\beta}\beta|\beta| + N'_{rr} r'|r'| \right. \\ &\quad \left. + \left(N'_{\beta\beta r}\beta + N'_{\beta rr} r'\right)\beta r'\right) \end{aligned} \tag{4}$$

where, X_H, Y_H, N_H are the longitudinal force, the lateral force, and the yaw moment acting on the ship's hull. X'_{vr} is predicted from Hasegawa's chart[9] and c_{TM} is determined from the model resistance tests discussed in Sect. 3.1. The hydrodynamic coefficients relative to β, i.e., Y'_β, $Y'_{\beta\beta}$, N'_β, and $N'_{\beta\beta}$, for the full load draft condition were determined from the captive model tests discussed in Sect. 3.3. The remaining hydrodynamic coefficients for the full load draft condition were determined using Kijima's regression model. For ballast draft conditions, all the hydrodynamic coefficients were determined using Kijima's regression model. In the free-running model experiments, the wind forces and moment were not considered as the experiments were carried out in fine weather.

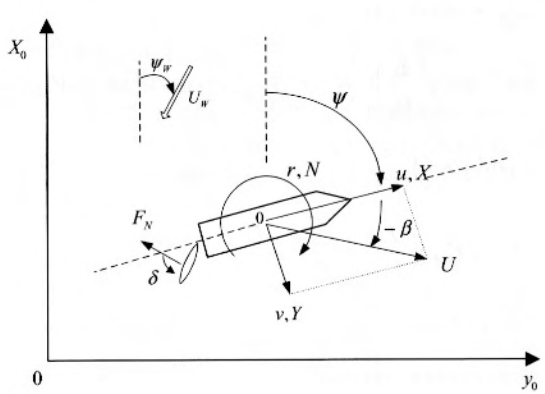

Fig. 7. Coordinate system

4.3 Mathematical model for the propeller thrust and torque

The mathematical model for the propeller thrust and torque is expressed as:

$$\begin{aligned} X_P &= (1 - t_P)(K_T)(\rho n^2 D_P^4) \\ Q_P &= -(\rho n^2 D_P^5)(K_q) \end{aligned} \tag{5}$$

$$\left.\begin{aligned} K_T &= a_1 + a_2 J + a_3 J^2 \\ K_q &= b_1 + b_2 J + b_3 J^2 \\ J &= (1 - w_M)u/(nD_P) \end{aligned}\right\} \tag{6}$$

The coefficients of the polynomial expressions for the propeller thrust and torque characteristics were previously determined from propeller open water tests and are shown in Table 4.

4.4 Mathematical model for the rudder forces and moment

When the rudder is operating behind the propeller, the rudder angle δ differs from the angle of attack α_R in the following way:

$$\alpha_R = \delta + \delta_0 + \beta_R \tag{7}$$

δ_0, the rudder angle when the lift force coefficient C_L becomes zero, is a correction for the flow asymmetry caused by the propeller slipstream. The propeller for the VLCC model turns to the right, when viewed from aft, and δ_0 is estimated to be +1.8° from the free-running experiments. β_R is the local drift angle at the given rudder position and is estimated as:

$$\beta_R = -\text{a}\tan 2(v_R, u_R) \tag{8}$$

The average inflow velocity to the rudder depends on the hull form, which induces wake (in the longitudinal direction) and a change of flow direction (in the transverse direction), and on the propeller, which accelerates the

Table 4. Coefficients of the propeller model

a_1	0.3883	b_1	0.0456
a_2	–0.2960	b_2	–0.0184
a_3	–0.1563	b_3	–0.0284

flow on the rudder surface. The rudder inflow velocities are modeled as:

$$u_R = \frac{\varepsilon u_p}{(1-s)}\sqrt{1-2(1-\eta\kappa)s+\{1-\eta\kappa(2-\kappa)\}s^2}$$
$$v_R = -\gamma_R(v + L_r r) \tag{9}$$

where $\varepsilon = \frac{1-w_R}{1-w_M}$, $s = 1-\frac{u_P}{nP}$, $\eta = \frac{D_P}{H}$, $u_p = (1-w_M)u$, and $\kappa = k_x/\varepsilon$.

The flow rectification coefficient γ_R and L_r, both of which depend on the hull form, were estimated for the same VLCC model, but with a mariner VecTwin rudder system and a different propeller.[2] The expression for u_R, the water velocity aft of the propeller, and the value of k_x, the propeller race amplification factor on the rudder surface, were validated for different VLCC and container ship models.[10] The expression for u_R is from impulse theory and k_x depends on the distance between the rudder and the propeller. Toda et al.[11] measured the wake for different regions in the stern of a series 60 ($C_b = 0.60$) model ship and showed that aft of the propeller plane there is a gradual increase in wake center-plane velocity and a relatively fast decay in transverse velocity, resulting in diffusion of the wake. This trend is usual for merchant ships with a conventional hull form, so $\varepsilon > 1.0$. The rudder forces and moment are expressed as:

$$X_R = -(1-t_R)C_N \sin\alpha_R\left(\frac{1}{2}\rho A_R(u_R^2+v_R^2)\right)\sin\delta$$
$$Y_R = -(1+a_H)C_N \sin\alpha_R\left(\frac{1}{2}\rho A_R(u_R^2+v_R^2)\right)\cos\delta$$
$$N_R = -(x_R + a_H x_H)C_N \sin\alpha_R\left(\frac{1}{2}\rho A_R(u_R^2+v_R^2)\right)\cos\delta \tag{10}$$

The asymmetric flow on the port and starboard sides of the rudder, induced by the rudder angle, not only results in lateral force $C_N \sin\alpha_R\left(\frac{1}{2}\rho A_R(u_R^2+v_R^2)\right)\cos\delta$ on the rudder (with application point x'_R), but also in an additional lateral force $a_H C_N \sin\alpha_R\left(\frac{1}{2}\rho A_R(u_R^2+v_R^2)\right)\cos\delta$ (with application point x_H) due to asymmetric flow on the port and starboard sides of the hull. For single-propeller/single-rudder ships, the values of the hull–rudder interaction coefficients have been published for ships having block coefficient in the range $0.50 < C_b < 0.83$.[12] For ships having $C_b \approx 0.81$, the range of a_H for model self-propulsion point was determined as $0.35 < a_H < 0.70$, the range of x'_H was determined as $-0.50 < x'_H < -0.30$, and $(1 - t_R) \approx 0.80$. The above ranges of values were determined for $\delta = \pm 25°$ and propeller revolutions of 24.0, 18.0, 12.0, and 6.0 RPS. The hull–rudder interaction coefficients (ε, a_H, x'_H) for the subject VLCC model were determined by tuning them in the above range using numerical simulations and comparing the results with the free-running trial results. During berthing maneuvers, when the propeller operates in all the four quadrants of the propeller revolution—ship speed plane, the coefficient a_H is expressed as a polynomial in terms of the advance coefficient (J). In this article, the simulations were carried out in the first quadrant of the propeller revolution—ship speed plane and at cruising speed (resulting in not much variation in the advance coefficient J), therefore a_H is assumed to be constant. In this article, t_R is assumed to be equal to t_P, and x_R is estimated from geometrical considerations.

Table 5. Coefficients of the rudder model

x'_H	–0.531
a_H	0.40
k_x	0.60
ε	1.70

The hull–rudder interaction coefficients for the full load draft for the VLCC model are shown in Table 5. The suitability of these coefficients for both the MS rudder and the MR rudder is discussed in Sect. 4.5.1. From 8000 twenty-foot equivalent unit (TEU) container ship model experiments, Eloot et al.[13] concluded that the rudder forces and interaction coefficients (a_H, x'_H) differ slightly for different drafts and under-keel clearances. Eloot et al.[13] also showed that there is an increase of flow induced by wake and the propeller slipstream at lower drafts and under-keel clearances, which results in smaller differences in rudder forces measured at ballast draft and loaded draft. For the subject VLCC, since all simulations were carried out in deep water, the same rudder model was used for both the full load and ballast conditions. The objective of this article was mainly to compare the performance of the two-rudder system, so the results from previously published values were tuned using the free-running model tests. It is expected that the comparison results would be similar even with exact values of these coefficients determined by elaborate model tests for both draft conditions.

4.5 Simulation of free-running model experiments

Several free-running maneuvering trials were conducted in a pond with both types of rudder system to validate the mathematical model. An underwater acoustic wave system was used to determine the model position in the experimental pond. The system consisted of two receivers fitted underwater and one transmitter fitted to the ship. The ship position was calculated by the time delay

of the acoustic signal received by the two receivers. The heading angle of the ship was measured by an onboard gyroscope. Zigzag tests and turning tests were carried out. During free-running experiments, the propeller revolutions were kept constant.

4.5.1 Simulation of maneuvering tests

The simulations of 20/20 zigzag tests for the MS and MR rudders are shown in Fig. 8. It can be seen that the simulations match the experimental results well. The experiment and simulation values for the overshoot angles and the time for first, second, and third overshoots compare favorably.

Several turning tests with both rudder systems were carried out. The simulations of 32° port turning tests with MS and MR rudders are shown in Fig. 9. It can be seen that the tactical diameter and the diameter of the turning circle for both rudders from the simulations match the experimental results well. For the advance data, the simulation results are slightly higher for both rudders compared to the experimental values. The advance data and tactical diameter for different turning tests are shown in Fig. 10. For turns to port, it can be seen that for both MS and MR rudders at higher rudder angles there is good similarity between simulation results and experimental values. For starboard turns, simulation results and experimental values match well for advance data for the MS rudder and for the tactical diameter for the MR rudder. However, for starboard turns, the simulation results and experimental values do not match well for advance data for the MR rudder and for the tactical diameter for the MS rudder. It may be

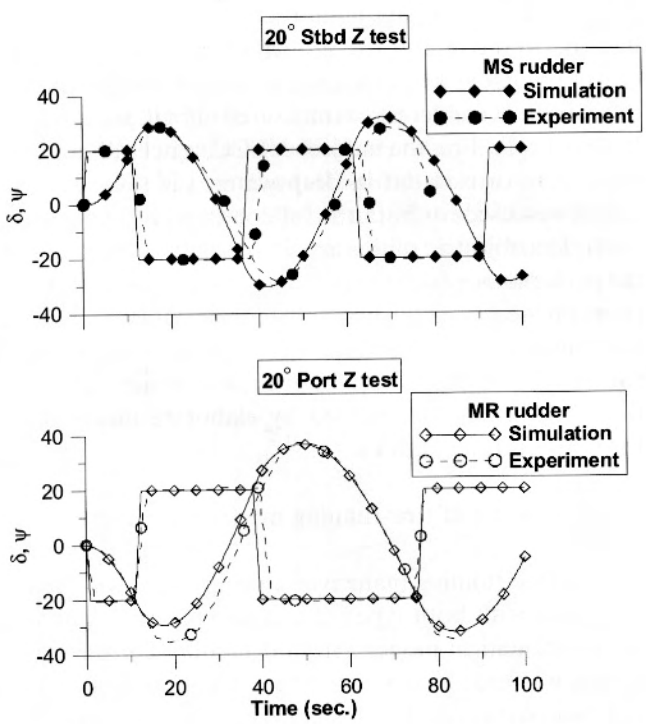

Fig. 8. Comparison of experimental and simulated zigzag (*Z*) test

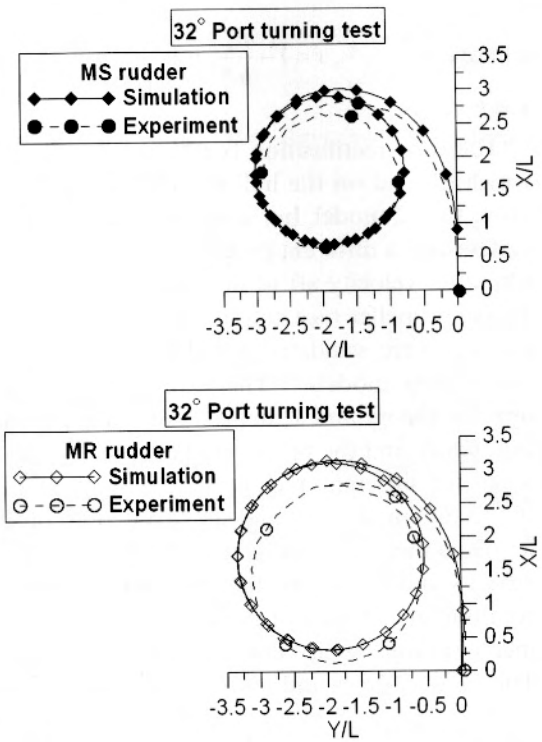

Fig. 9. Comparison of trajectory between experiment and simulation (turning test)

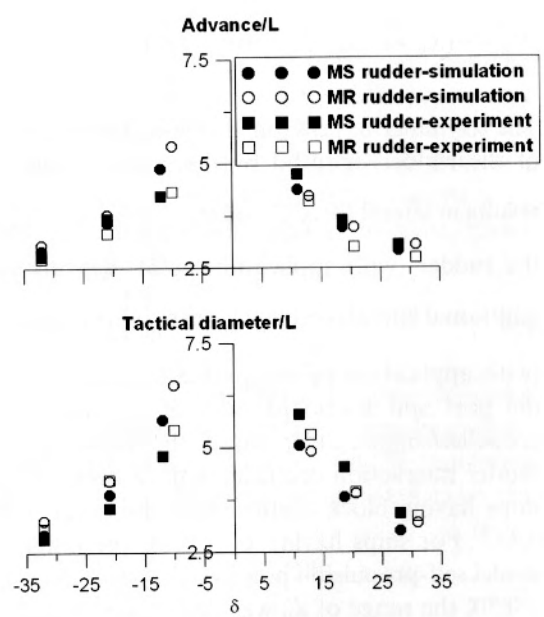

Fig. 10. Comparison of advance and tactical diameter between experiment and simulation (turning test)

noted that in free-running tests, it is very difficult to establish exact initial values of surge, sway, and yaw speeds. The above differences are caused by the slightly different initial conditions of the experiments. From a comparison of the free-running experiments and simulations, the MMG model is considered suitable for use in numerical simulations to compare the performances of MS and MR rudders.

5 Full-scale simulations

The subject VLCC model was fabricated for experimental purposes only and does not have a known full-scale equivalent. As most VLCCs in operation have a length in the range of 300–320 m, the length and breadth were scaled up from model values using a scale ratio of 1:78.75. Accommodation superstructure, which is located aft, has a significant influence on the wind force coefficient. To estimate the ship's depth and the area of the accommodation superstructure, data from existing VLCCs in service were considered. The scaled-up particulars of the VLCC are shown in Table 6.

5.1 Aerodynamic forces and moments

The aerodynamic forces and moment induced by gusting winds are considered in this article. The expressions of the forces and the moment induced by the wind are:

$$\left.\begin{aligned} X_W &= \frac{1}{2}\rho_A A_T U_A^2 C_X(\psi_A) \\ Y_W &= \frac{1}{2}\rho_A A_L U_A^2 C_Y(\psi_A) \\ N_W &= \frac{1}{2}\rho_A A_L U_A^2 L C_N(\psi_A) \end{aligned}\right\} \tag{11}$$

where $C_X(\psi_A)$, $C_Y(\psi_A)$, $C_N(\psi_A)$ are the aerodynamic drag coefficients.

Table 6. Principal particulars of full-scale VLCC ship

Length (m)	315.00
Breadth (m)	52.50
Depth (m)	30.50
Loaded draft	
Even keel (m)	18.90
C_b	0.817
Ballast draft	
Forward (m)	6.30
Aft (m)	11.50
C_b	0.776
Superstructure	
Transverse area (m^2)	600
Longitudinal area (m^2)	750

Fujiwara's[14] regression formula was selected to estimate the aerodynamic drag coefficients. Fujiwara's regression formulae were developed for new ship types such as large PCCs, LNG carriers, container ships, VLCCs, and passenger ships. Hasegawa et al.[15] showed that the aerodynamic drag coefficients estimated by Fujiwara's regression formula are comparable to the results of wind tunnel experiments on a PCC carried out for wind encounter angles in the range 0°–60° by Matsumuto et al.[16]

Fujiwara's regression formula not only considers the absolute wind area but also the distribution of wind area when estimating aerodynamic drag coefficients. Numerical simulations comparing fuel efficiency and maneuvering characteristics were carried out at full scale.

The wind area particulars for loaded and ballast drafts are shown in Table 7. It can be seen that, at loaded draft, the wind area is distributed aft, whereas at ballast draft, the centre of wind area, though remaining aft, shifts nearer to midship. The wind force coefficients for simulations were calculated for ballast draft and loaded draft and are shown in Fig. 11 as functions of the encounter wind angle.

Gusting wind was generated using the Davenport spectrum[17]:

$$\frac{1}{2\pi}S_z\left(\frac{\omega}{2\pi}\right).d\omega = 4.0\kappa_W U_W^2 \frac{x}{(1+x^2)^{4/3}}dx \tag{12}$$

where $x = \dfrac{1200\omega}{2\pi U_W}$ and $\dfrac{\omega}{2\pi U_W}$ is in cycles per meter.

The fluctuating wind velocity is obtained as:

$$U_{GW}(t) = \sum_{i=1}^{N} b_i \sin(\omega_i t + \delta_i) \tag{13}$$

where b_i is the amplitude of gustiness and δ_i is the phase angle of gustiness.

The amplitude of the ith wind component is determined under linear theory as:

$$b_i = \sqrt{2S_z(\omega_i)\Delta\omega_i} \tag{14}$$

Table 7. Distribution of windage area of the VLCC ship

	Draft condition	
	Ballast	Loaded
Transverse area (m^2)	1870.5	1209
Longitudinal area (m^2)	7770.4	4520
Center of longitudinal area (m) (Aft: –, Fwd: +)	−5.84	−20.16

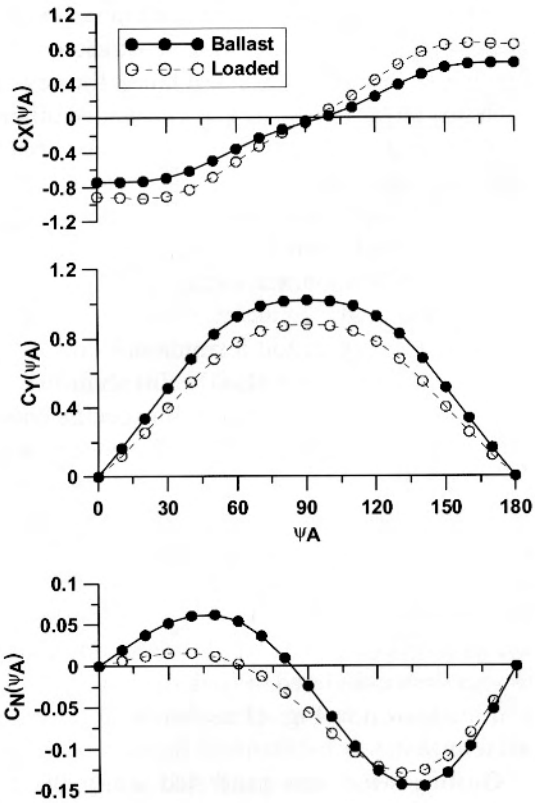

Fig. 11. Aerodynamic drag coefficients

Here, $\Delta\omega_i$ is the discretized interval of the ith wind component. To avoid repeating patterns of gusting wind, non-evenly distributed discrete frequencies were used. The phase angle δ_i was generated by a random number. The maximum wind speed used for simulation was 24.0 m/s and the effective frequency range for this wind speed was $\omega = 0$–10 radians/s.

5.2 Constant torque simulation of the main engine

Hasegawa et al.[15] showed that at cruising speed, by assuming constant torque operation of the main engine, the variation in propeller revolutions can be accurately simulated; in this article, the constant torque operation of the main engine is considered for simulation. The relation between the changes in propeller revolutions and the propeller torque can be expressed as[18]:

$$2\pi(J_{PP} + \Delta J_{PP})\dot{n} + \rho n^2 D_P^5 K_q = Q_P \tag{15}$$

The added polar moment of inertia (ΔJ_{PP}) is taken as 25% of the propeller's polar moment of inertia in air.[19] The relation between the main engine torque and the propeller torque is[20]:

$$g_R \eta_t \eta_R Q_E = Q_P \tag{16}$$

Table 8. Speed simulation for the MR rudder and the MS rudder

Ship draft (m)	Propeller revolutions (RPM)	Mean speed (m/s)	Main engine torque (kN-m)
8.90 (ballast)	58.70	8.01	1900.00
18.90 (loaded)	56.14	6.91	1900.00

where g_R is the gear ratio, η_t is the shaft transmission efficiency, and η_R is the relative rotative efficiency.

For the subject VLCC, the gear ratio is 1.0. In this article, the performances of the MR and MS rudders were compared using the same VLCC. Because the propeller and shaft system are the same for both rudder types, η_t for both systems is assumed to be 1.0.

When the rudder angle is given, there is a drift, and the ship's drift induces a variation in wake fraction and increases the drag; using this relation and the constant torque operation of the engine, the changes in propeller revolutions can be simulated. If the main engine torque and shaft revolutions are known, the power and fuel consumption can be calculated as follows:

$$\begin{aligned} &\text{Power} = 2\pi n Q_E \\ &\text{Fuel consumption} = SFOC * Power * Time \end{aligned} \tag{17}$$

It may be noted that for constant torque, the specific fuel oil consumption (SFOC) for diesel engines can be assumed to be constant. In this work, the value assumed is 165.0 g/kWh.[21] The steady ship speed, propeller revolutions, and constant main engine torque used in the simulations are shown in Table 8.

5.3 Maneuvering simulation without external forces

Zigzag and turning test simulations without external forces were carried out for both the MS rudder and the MR rudder at constant main engine torque. The overshoot angle from the zigzag tests and advance and transfer data from the turning tests were calculated from the simulation results. The values are shown in Tables 9 and 10 for the full load condition.

Even with a smaller rudder area, the MS rudder was found to be superior to the MR rudder. The results shown here are for the full load condition; understandably, the differences become more marked for the ballast condition, in which the MR rudder loses control area because of the lower waterline. These factors will have much influence on ship safety while it is underway in narrow channels at reduced speeds.

Table 9. Overshoot angle for zigzag simulation

	MS rudder		MR rudder	
Overshoot	Time (s)	Angle (°)	Time (s)	Angle (°)
10° port zigzag test				
First	125	3.7	146	4.4
Second	365	12.2	447	17.4
10° starboard zigzag test				
First	139	6.7	172	8.4
Second	379	7.1	461	10.2
20° port zigzag test				
First	137	9.4	162	10.8
Second	392	15.5	474	20.5
20° starboard zigzag test				
First	144	12.2	174	14.1
Second	405	12.4	485	16.0

Table 10. Advance and transfer data for turning tests

	Advance/L	Tactical diameter/L
MS rudder		
35° port	3.1	3.1
35° starboard	2.9	3.0
MR rudder		
35° port	3.4	3.4
35° starboard	3.2	3.3

5.4 Course-keeping simulations in windy conditions

With the above model, course-keeping simulations were carried out under gusting wind conditions for various wind directions. For the simulations, maximum permissible rudder angle and rudder rate limiters were used, i.e., $|\delta_{max}| = 35°$ and $|\dot{\delta}_{max}| = 2.5°/s$. To understand the effect of the wind area, the results for the ballast draft and loaded draft cases are discussed separately.

5.4.1 Tuning of autopilot coefficients

A proportional–integral–differential (PID) type autopilot was used for course-keeping simulations. The autopilot was based on the following equation:

$$\delta = K_P((\psi_d - \psi) - T_d r) + K_i(y_d - y) \tag{18}$$

To compare the performance of the two different rudder systems, an appropriate selection of the autopilot coefficients suitable for both the rudder systems is necessary. Optimizing the autopilot coefficients for various conditions is a separate research in itself. In this study, the objective is to determine a set of autopilot coefficients which are not biased towards either MR rudder or MS rudder system and use it for simulation purposes. In this section, we will explain how the autopilot coefficients are determined. The explanation is for ballast draft. A steady wind speed of 24.0 m/s and beam wind direction was assumed.

It is convenient to define a certain evaluation function to tune the autopilot coefficients. An evaluation function was defined for tuning the regulator gain for both types of rudders using the non-linear ship model. In the ship model, the main engine is considered to operate in constant torque condition, so any variation in drag also induces variation in propeller revolution. Since the straight distance traveled and propeller revolution varies under external disturbance, we defined the evaluation function as straight distance traveled for unit fuel consumed. A higher value of the evaluation function indicates good performance of the ship. However, the evaluation function is neither sensitive to rudder's oscillatory motions nor to the ship's off-centerline deviation both of which also influences ship's performance. Identification of a universal evaluation function incorporating these parameters would be ideal. In this study, the evaluation function is used for selecting the coefficient K_P, while the coefficients T_d and K_i were determined using different criteria, which are described later.

Firstly, we assume $T_d = 10$, $K_i = 0$ and carried out simulations by varying K_P. The results are shown in Fig. 12. The evaluation function is maximum in the region $1 \le K_p \le 100$ for both MS and MR rudder. This time we chose $K_p = 5$ from this region.

The major influence of T_d appears on the frequency of rudder motion. We selected T_d based on rudder oscillation. We know that for T_d beyond certain number, rudder movement is oscillating. This oscillation increases ship's resistance and may also induce mechanical failure in rudder system. We checked this behavior for two typical cases, and the simulation results are shown in Fig. 13. For $T_d = 10$, the rudder angle becomes steady at –8.7°. However for $T_d = 100$, the rudder is oscillating

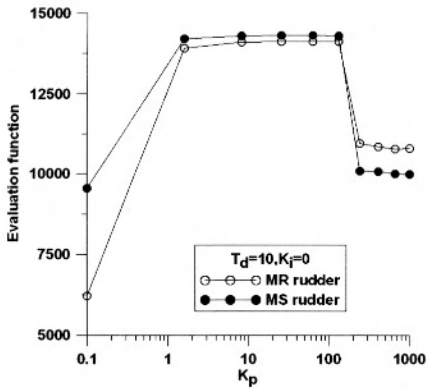

Fig. 12. Variation of evaluation function showing the influence of K_P (ballast draft)

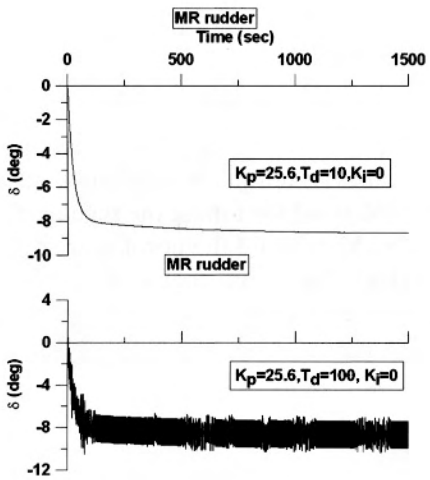

Fig. 13. Time series of rudder angle showing the influence of T_d (ballast draft)

about mean angle –8.7°. MS rudder also shows similar behavior. This time we chose T_d = 10 from the above consideration.

Finally, we determine the coefficient K_i. The purpose of K_i is to reduce ship's off-centerline deviation. Higher is the value of K_i, smaller is the off-centerline deviation. The off-centerline deviation should be small enough, but the integral control will be effective when the ship's off-centerline deviation exceeds some permissible value. Here we set the limit of off-centerline deviation to be one ship length per 5,000 secs. We used K_P and T_d values determined above and carried out simulations by varying K_i. The results are shown in Fig. 14. We chose $K_i = 10^{-3}$, where the off-centerline deviation is around one ship length.

In case of loaded draft, we determined the coefficients in similar way and the results are K_p = 10.0, T_d = 10.0, $K_i = 10^{-3.0}$.

For each draft condition, the same set of autopilot coefficients were used for course-keeping simulations for

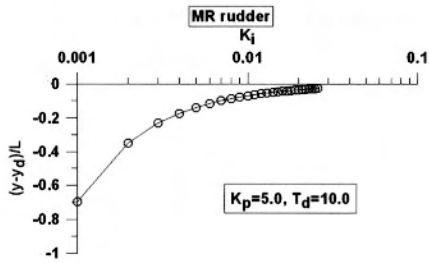

Fig. 14. Variation of ship's off-centerline deviation showing influence of K_i (ballast draft)

both MS and MR rudders and we regard there is no difference caused by autopilot parameters for both rudder system.

5.4.2 Simulations at loaded draft

Simulations were carried out for various wind speeds and wind heading angles with both rudder systems. The mean values of rudder angle, speed, main engine power, and other data were determined and the results are shown in Fig. 15. The autopilot coefficients were suitable for both the MS and MR rudders at their respective loading conditions.

The simulation results are reasonable because for quartering and following winds the fuel efficiency was higher due to the additional propelling thrust from the wind. Although the MS rudder had a smaller area, the angle required by the MS rudder was lower compared to the MR rudder for all cases; however, because the windage area was lower at loaded draft, the maximum rudder angle was within 6°. Although the MS rudder is superior, the difference in performance between the MS and MR rudders is not significant.

5.4.3 Simulations at ballast draft

Simulations were carried out for various wind angles and wind speeds and a summary of the results is shown in Fig. 16. In ballast draft, it can be seen that the influence of the wind is significant. To maintain course, the ship undergoes large drift motions. For wind speeds of 18.0 and 24.0 m/s and wind heading angles between 45° and 105°, the ship speed for the MS rudder was higher than that for the MR rudder. The maximum angle for the MS rudder was about 5°, while for the MR rudder it was about 9°; the increased angle contributes to extra drag for the MR rudder. To understand these phenomena more clearly, a comparison of time series of motion for both rudder types for a particular wind condition is shown in Fig. 17. From the figure it can be seen that the

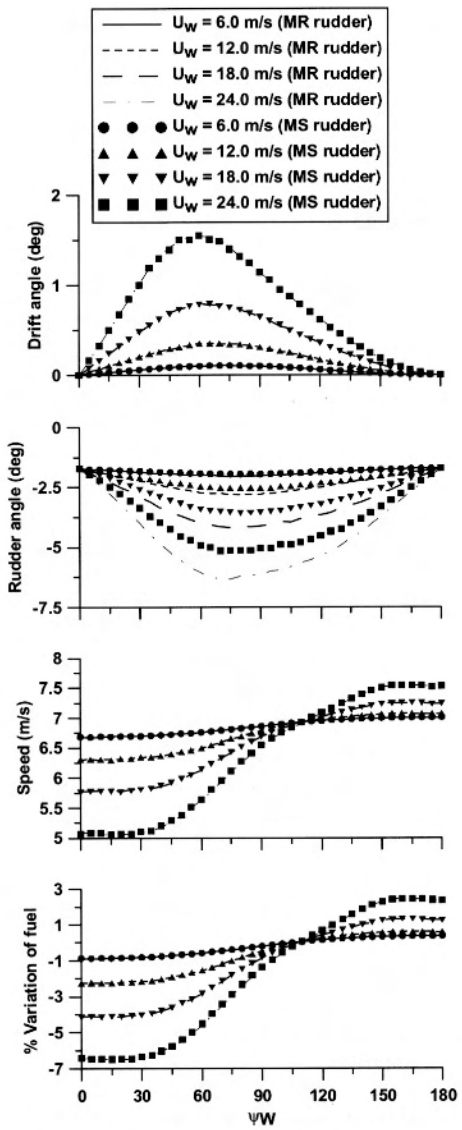

Fig. 15. Comparison of performance for various wind speeds and directions at loaded draft. The percentage variation of fuel means variation of fuel consumed between wind and without wind condition

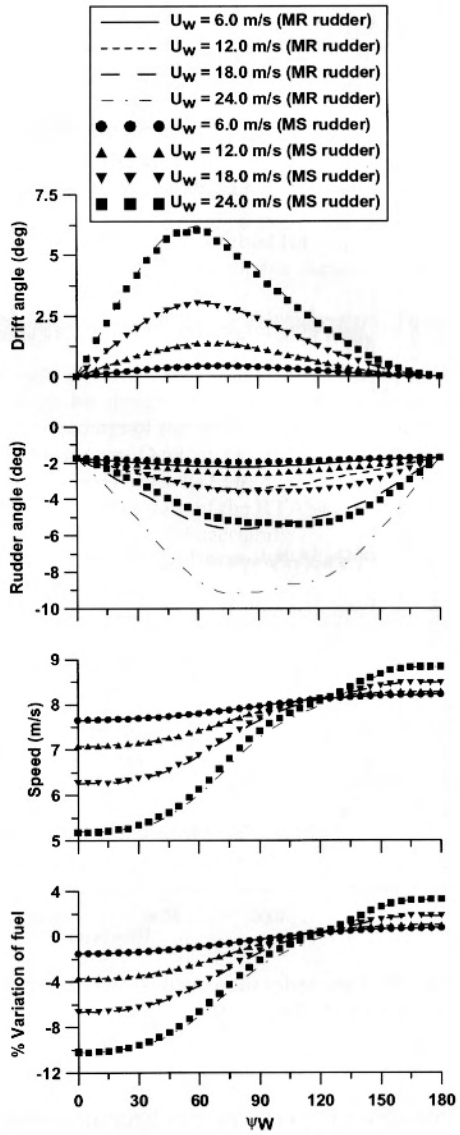

Fig. 16. Comparison of performance for various wind speeds and directions at ballast draft. The percentage variation of fuel means variation of fuel consumed between wind and without wind condition

drop in speed for the MS rudder is less than that for the MR rudder; the difference in speed is due to the difference in rudder angle.

A comparison of fuel consumption for the same time of travel is shown in Table 11 for both loaded and ballast drafts; the conditions were a wind speed of 24.0 m/s and a wind encounter angle of 90°. It can be seen that in the same time, at both loaded and ballast draft, the ship fitted with the MS rudder covers a longer distance while consuming almost the same amount of fuel as the ship fitted with the MR rudder. In the ballast draft condition, due to the combined effects of the increase in wind area and the loss of control surface of the MR rudder, the

Table 11. Comparison of fuel efficiency of MS rudder and MR rudder for a simulation lasting 20000 s

Draft/rudder	Fuel consumed (MT)	Distance/L
Ballast draft (8.90 m)		
MS	10.5	472.1
MR	10.4	462.5
Full draft (18.90 m)		
MS	10.1	416.4
MR	10.1	415.10

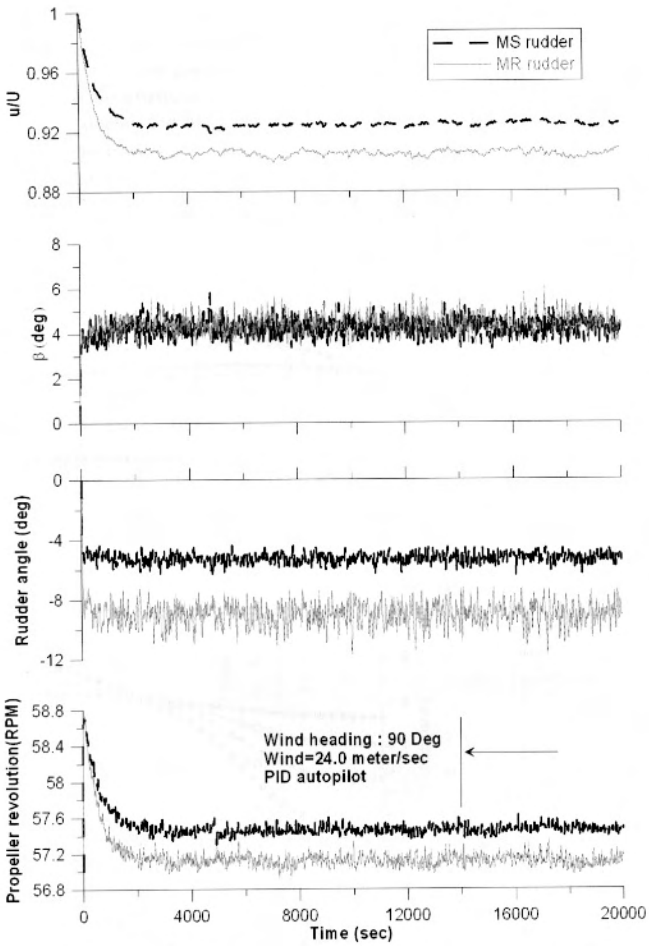

Fig. 17. Time series showing difference in performance of MR and MS rudder (Ballast draft)

difference in performance becomes more prominent, i.e., about 2.0%. The simulation results clearly indicate the positive influence of the mariner Schilling rudder on fuel consumption performance under windy conditions.

6 Conclusions

The performances of the MS rudder and the MR rudder under various loading and gusting wind conditions were compared. The superiority of the MS rudder over the MR rudder from the viewpoint of the optimum arrangement and their performance in full-scale conditions was discussed. It was seen that without any external force acting, for the same main engine torque, the speed and the propeller revolutions of ships fitted with MR rudders and MS rudders were same. At constant engine torque, the maneuverability of the ship with an MS rudder was superior to that of the ship with an MR rudder. Additionally, during course-keeping tests at various wind encounter angles and various gusting winds, the fuel efficiency of the ship fitted with the MS rudder was higher than that of the ship fitted with the MR rudder. During course keeping under windy conditions, the ship fitted with an MS rudder covered a greater distance per unit amount of fuel consumed; this difference was more prominent for the ballast draft condition. The rudder model developed for the full load condition was also used to compare the performances of the MS and MR rudders in the ballast draft condition. Since existing VLCCs exhibit better maneuverability for ballast draft than for loaded draft, the trend of the results would not be expected to be different if an accurate rudder model were to be developed for the ballast draft condition. Although we have been able to qualitatively develop the ship model by comparison with free-running model experiments, it should be recognized that quantitative prediction of the rudder model requires more elaborate experiments. With regard to the direction of future work, it would be interesting to see if the difference in performance of the two rudders increased or decreased by developing a more accurate model of the rudder system in both loaded and ballast draft conditions. Also of interest is the influence of scale effects on the mathematical model and the resulting influence on the full-scale performance.

References

1. Hasegawa K, Kang DH, Sano M, et al (2006) A study on improving the course-keeping ability of a pure car carrier in windy conditions. J Mar Sci Technol 11:76–87
2. Hasegawa K, Kang DH, Sano M, et al (2006) Study on the maneuverability of a large vessel installed with a mariner type Super VecTwin rudder. J Mar Sci Technol 11:88–99
3. Spyrou K (1995) Yaw stability of ships in steady wind. Schiffstechnik Bd 42-1995/ Ship Technol Res 42:21–30
4. Tachi K, Endo M (1995) Estimated manoeuvrability of T.S. *Wakashio-maru-I*—wind tunnel test and rudder open test. J Jpn Inst Navig 94:17–26
5. Hadler JB, Cheng HM (1965) Analysis of experimental wake data in way of the propeller plane of single- and twin-screw ship models. Trans SNAME 73:287–414
6. Oosterveld MWC (1978) Appendix to the report of the performance committee, part-I. In: Oosterveld MWC, Netherlands Ship Model Basin (eds) Proceedings of the 15th international towing tank conference. Netherlands Ship Model Basin, Wageningen, Netherlands
7. Kijima K, Nakiri Y (2002) On the practical prediction method for ship maneuvering characteristics (in Japanese). Trans West Jpn Soc Naval Archit 105:21–31
8. Det Norske Veritas (1985) Hull equipment and appendages: stern frames, rudders and steering gears. Rules for classification of steel ships, Part 3, Chapter 3, Section 2:2–19, Det Norske Veritas, Hovik, Norway
9. Hasegawa K (1980) On a performance criterion for autopilot navigation. J Kansai Soc Naval Archit 178:93–104

10. Yoshimura Y, Nomoto K (1978) Modeling of manoeuvring behaviour of ships with the propeller idling, boosting and reversing. J Soc Naval Archit Jpn 144:57–69
11. Toda Y, Stern F, Tanaka I, Patel VC (1990) Mean flow measurements in the boundary layer and wake of a series 60 $C_B = 0.6$ model ship with and without a propeller. J Ship Res 34:225–252
12. Kobayashi E, Kagemoto H, Furukawa Y (1995) Mathematical models of maneuvering motions (in Japanese). In: Research on ship maneuverability and its application to ship design, Proceedings of the 12th marine dynamic symposium. Society of Naval Architects of Japan, Tokyo, pp 23–89
13. Eloot K, Vantorre M, Delefortrie G (2006) Prediction of ship manoeuvrability of an 8000 TEU containership in deep and shallow water: mathematical modelling and captive model testing. In: Proceedings of MARSIM 2006. Maritime Institute Willem Barentsz, Terschelling, The Netherlands, pp M.3.1–M.3.9
14. Fujiwara T, Ueno M, Nimura T (1998) Estimation of wind forces and moments acting on ships (in Japanese). J Soc Naval Archit Jpn 183:77–90
15. Hasegawa K, Nagarajan V, Kang DH (2006) Performance evaluation of Schilling rudder and mariner rudder for pure car carriers under windy conditions. MARSIM 2006, Terschelling, The Netherlands, pp M.5.1–M.5.10
16. Matsumoto K, Tanaka Y, Hirota K, et al (2003) Reduction of wind force acting on ships (in Japanese). J Kansai Soc Naval Archit 240:115–121
17. Davenport AG (1961) The spectrum of horizontal gustiness near the ground in high winds. Q J R Meteorol Soc 87:194–211
18. Hirano M (1980) On a calculation method for ship maneuvering motion at the initial design phase (in Japanese). J Soc Naval Archit Jpn 147:144–153
19. Nippon Kaiji Kyokai (1984) Guide to ship vibration. Tokyo, pp 63–66
20. Naito S, Nakamura S (1985) Prediction of speed loss in waves and its implication on design. In: Theory and practice of marine design, Proceedings of the second international marine systems design conference. Dept of Ocean Engineering, The Technical University of Denmark, Lyngby, Denmark
21. Sulzer (2000) Primary engine data of the RTA84T-D. Wartsila NSD Sulzer Ltd., Winterthur, Switzerland